

Photoacoustic imaging velocimetry for flow-field measurement

Songbo Ma, Sihua Yang, and Da Xing*

MOE Key Laboratory of Laser Life Science & Institute of Laser Life Science, College of Biophotonics,
South China Normal University, Guangzhou 510631, China

*xingda@scnu.edu.cn

Abstract: We present the photoacoustic imaging velocimetry (PAIV) method for flow-field measurement based on a linear transducer array. The PAIV method is realized by using a Q-switched pulsed laser, a linear transducer array, a parallel data-acquisition equipment and dynamic focusing reconstruction. Tracers used to track liquid flow field were real-time detected, two-dimensional (2-D) flow visualization was successfully reached, and flow parameters were acquired by measuring the movement of the tracer. Experimental results revealed that the PAIV method would be developed into 3-D imaging velocimetry for flow-field measurement, and potentially applied to research the security and targeting efficiency of optical nano-material probes.

©2010 Optical Society of America

OCIS codes: (170.5120) Photoacoustic imaging; (170.0110) Imaging systems; (170.3010) Image reconstruction techniques; (120.7250) Velocimetry.

References and links

1. R. I. Siphanto, K. K. Thumma, R. G. Kolkman, T. G. van Leeuwen, F. F. de Mul, J. W. van Neck, L. N. van Adrichem, and W. Steenbergen, "Serial noninvasive photoacoustic imaging of neovascularization in tumor angiogenesis," *Opt. Express* **13**(1), 89–95 (2005).
2. Q. Zhang, Z. Liu, P. R. Carney, Z. Yuan, H. Chen, S. N. Roper, and H. Jiang, "Non-invasive imaging of epileptic seizures in vivo using photoacoustic tomography," *Phys. Med. Biol.* **53**(7), 1921–1931 (2008).
3. C. K. Liao, S. W. Huang, C. W. Wei, and P. C. Li, "Nanorod-based flow estimation using a high-frame-rate photoacoustic imaging system," *J. Biomed. Opt.* **12**(6), 064006–064009 (2007).
4. G. F. Lungu, M. L. Li, X. Xie, L. V. Wang, and G. Stoica, "In vivo imaging and characterization of hypoxia-induced neovascularization and tumor invasion," *Int. J. Oncol.* **30**(1), 45–54 (2007).
5. Z. Yuan, C. Wu, H. Zhao, and H. Jiang, "Imaging of small nanoparticle-containing objects by finite-element-based photoacoustic tomography," *Opt. Lett.* **30**(22), 3054–3056 (2005).
6. Z. Yuan, Q. Wang, and H. Jiang, "Reconstruction of optical absorption coefficient maps of heterogeneous media by photoacoustic tomography coupled with diffusion equation based regularized Newton method," *Opt. Express* **15**(26), 18076–18081 (2007).
7. X. Wang, Y. Pang, G. Ku, X. Xie, G. Stoica, and L. V. Wang, "Noninvasive laser-induced photoacoustic tomography for structural and functional in vivo imaging of the brain," *Nat. Biotechnol.* **21**(7), 803–806 (2003).
8. J. J. Niederhauser, M. Jaeger, R. Lemor, P. Weber, and M. Frenz, "Combined ultrasound and optoacoustic system for real-time high-contrast vascular imaging in vivo," *IEEE Trans. Med. Imaging* **24**(4), 436–440 (2005).
9. R. A. Kruger, K. D. Miller, H. E. Reynolds, W. L. Kiser, Jr., D. R. Reinecke, and G. A. Kruger, "Breast cancer in vivo: contrast enhancement with thermoacoustic CT at 434 MHz-feasibility study," *Radiology* **216**(1), 279–283 (2000).
10. S. Manohar, S. E. Vaartjes, J. C. van Hespren, J. M. Klaase, F. M. van den Engh, W. Steenbergen, and T. G. van Leeuwen, "Initial results of in vivo non-invasive cancer imaging in the human breast using near-infrared photoacoustics," *Opt. Express* **15**(19), 12277–12285 (2007).
11. M. Pramanik, G. Ku, C. H. Li, and L. V. Wang, "Design and evaluation of a novel breast cancer detection system combining both thermoacoustic (TA) and photoacoustic (PA) tomography," *Med. Phys.* **35**(6), 2218–2223 (2008).
12. S. A. Ermilov, T. Khamapirad, A. Conjusteau, M. H. Leonard, R. Lacewell, K. Mehta, T. Miller, and A. A. Oraevsky, "Laser optoacoustic imaging system for detection of breast cancer," *J. Biomed. Opt.* **14**(2), 024007 (2009).
13. L. Li, R. J. Zemp, G. Lungu, G. Stoica, and L. V. Wang, "Photoacoustic imaging of lacZ gene expression in vivo," *J. Biomed. Opt.* **12**(2), 020504 (2007).
14. R. O. Esenaliev, I. V. Larina, K. V. Larin, D. J. Deyo, M. Motamedi, and D. S. Prough, "Optoacoustic technique for noninvasive monitoring of blood oxygenation: A feasibility study," *Appl. Opt.* **41**, 4722–4731 (2002).

15. H. F. Zhang, K. Maslov, G. Stoica, and L. V. Wang, "Functional photoacoustic microscopy for high-resolution and noninvasive in vivo imaging," *Nat. Biotechnol.* **24**(7), 848–851 (2006).
16. J. Laufer, C. Elwell, D. Delpy, and P. Beard, "In vitro measurements of absolute blood oxygen saturation using pulsed near-infrared photoacoustic spectroscopy: accuracy and resolution," *Phys. Med. Biol.* **50**(18), 4409–4428 (2005).
17. M. L. Li, J. T. Oh, X. Y. Xie, G. Ku, W. Wang, C. Li, G. Lungu, G. Stoica, and L. V. Wang, "Simultaneous molecular and hypoxia imaging of brain tumors in vivo using spectroscopic photoacoustic tomography," *Proc. IEEE* **96**(3), 481–489 (2008).
18. S. Hu, B. Rao, K. Maslov, and L. V. Wang, "Label-free photoacoustic ophthalmic angiography," *Opt. Lett.* **35**(1), 1 (2010).
19. E. I. Galanzha, E. V. Shashkov, T. Kelly, J. W. Kim, L. Yang, and V. P. Zharov, "In vivo magnetic enrichment and multiplex photoacoustic detection of circulating tumour cells," *Nat. Nanotechnol.* **4**(12), 855–860 (2009).
20. P. Ephrat, M. Roumeliotis, F. S. Prato, and J. J. L. Carson, "3D photoacoustic imaging of a moving target," *Proc. SPIE* **7177**, 71770W–1-9 (2009).
21. P. Ephrat, M. Roumeliotis, F. S. Prato, and J. J. L. Carson, "Four-dimensional photoacoustic imaging of moving targets," *Opt. Express* **16**(26), 21570–21581 (2008).
22. D. W. Yang, D. Xing, S. H. Yang, and L. Z. Xiang, "Fast full-view photoacoustic imaging by combined scanning with a linear transducer array," *Opt. Express* **15**(23), 15566–15575 (2007).
23. L. M. Nie, D. Xing, and S. H. Yang, "In vivo detection and imaging of low-density foreign body with microwave-induced thermoacoustic tomography," *Med. Phys.* **36**(8), 3429–3437 (2009).
24. C. K. Liao, M. L. Li, and P. C. Li, "Optoacoustic imaging with synthetic aperture focusing and coherence weighting," *Opt. Lett.* **29**(21), 2506–2508 (2004).
25. W. J. Welch, X. Deng, H. Snellen, and C. S. Wilcox, "Validation of miniature ultrasonic transit-time flow probes for measurement of renal blood flow in rats," *Am. J. Physiol. Renal Physiol.* **268**, F175–F178 (1995).
26. X. Jin, and L. V. Wang, "Thermoacoustic tomography with correction for acoustic speed variations," *Phys. Med. Biol.* **51**(24), 6437–6448 (2006).
27. R. J. Zemp, L. Song, R. Bitton, K. K. Shung, and L. V. Wang, "Realtime photoacoustic microscopy in vivo with a 30-MHz ultrasound array transducer," *Opt. Express* **16**(11), 7915–7928 (2008).
28. H. Golster, M. Lindén, S. Bertuglia, A. Colantuoni, G. Nilsson, and F. Sjöberg, "Red blood cell velocity and volumetric flow assessment by enhanced high-resolution laser Doppler imaging in separate vessels of the hamster cheek pouch microcirculation," *Microvasc. Res.* **58**(1), 62–73 (1999).
29. D. E. Goertz, J. L. Yu, R. S. Kerbel, P. N. Burns, and F. S. Foster, "High-frequency 3-D color-flow imaging of the microcirculation," *Ultrasound Med. Biol.* **29**(1), 39–51 (2003).
30. L. Sandrin, S. Manneville, and M. Fink, "Ultrafast two-dimensional ultrasonic speckle velocimetry: A tool in flow imaging," *Appl. Phys. Lett.* **78**(8), 1155–1157 (2001).
31. H. B. Kim, J. Hertzberg, C. Lanning, and R. Shandas, "Noninvasive measurement of steady and pulsating velocity profiles and shear rates in arteries using echo PIV: in vitro validation studies," *Ann. Biomed. Eng.* **32**(8), 1067–1076 (2004).
32. H. Fang, and L. V. Wang, "M-mode photoacoustic particle flow imaging," *Opt. Lett.* **34**(5), 671–673 (2009).
33. A. De La Zerdá, C. Zavaleta, S. Keren, S. Vaithilingam, S. Bodapati, Z. Liu, J. Levi, B. R. Smith, T. J. Ma, O. Oralkan, Z. Cheng, X. Y. Chen, H. J. Dai, B. T. Khuri-Yakub, and S. S. Gambhir, "Carbon nanotubes as photoacoustic molecular imaging agents in living mice," *Nat. Nanotechnol.* **3**(9), 557–562 (2008).
34. J. W. Kim, E. I. Galanzha, E. V. Shashkov, H. M. Moon, and V. P. Zharov, "Golden carbon nanotubes as multimodal photoacoustic and photothermal high-contrast molecular agents," *Nat. Nanotechnol.* **4**(10), 688–694 (2009).

1. Introduction

Photoacoustic imaging (PAI) combines high optical contrast with fine ultrasound resolution, and it provides a promising hybrid imaging modality for scientific research and clinic diagnosis [1–6]. PAI has been employed to image vasculature structure [7,8], detect breast tumors [9–12], track molecular probes [13], measure oxygen saturation [14–16], perform molecular and function imaging [7,17], research ophthalmic angiography [18] and count cell [19].

Ephrat et al. developed a 3-D photoacoustic imaging system to image moving target based on a sparse array and iterative imaging reconstruction [20,21]. Liao et al. measured nano-based flow speed with photoacoustic wash-in technology [3]. In this paper, real-time photoacoustic imaging technology was used to measure flow field. Moving tracers used to track flow field were real-timely detected and the speed of flow field was acquired by measuring the movement of the tracer with continuous PA images. This speed measuring method is referred as photoacoustic imaging velocimetry.

The method is realized by using a Q-switched pulsed laser, a linear transducer array, a parallel data-acquisition equipment and dynamic focusing reconstruction. In this imaging system, the linear transducer array is used as a staring array. For each laser pulse, PA signals

are collected by the 64-channel staring array, and then temporarily stored in a buffer memory module of the data-acquisition equipment. After a completed data is acquired, the data is transferred to a PC, and PA images are reconstructed off-line with dynamic focusing algorithm. The frame rate of the PAIV system is 15 Hz, which is limited by the laser pulse repetition frequency. With the PAIV system, PA signals of the tracer moving in flow field can be captured real-timely, 2-D flow visualization can be successfully recorded with continuous PA images, and flow parameters can be acquired by measuring the movement of the tracer. To verify the capability of flow visualization and flow-field measurement of the imaging system, phantoms made of wood block and Indian ink were constructed to track flow field. Experimental results validated that the PAIV system has the ability of two-dimensional flow visualization for flow field measurement. To our knowledge, this is the first report of flow field measurement with photoacoustic imaging velocimetry method.

2. Methods

The schematic of the PAIV system is shown in Fig. 1(a). A Q-Switched Nd: YAG laser (LOTIS TII Ltd, Minsk, Belarus) is used as excitation source, which operates at 1064 nm with pulse duration of 10 ns and pulse repetition rate of 15 Hz. The laser is expanded by a concave lens and then homogenized by a piece of ground glass, and the incident energy density is controlled below 20 mJ/cm². The incident laser beam has a diameter of 2.5 cm. PA signals are detected by the 64-element linear transducer array. Each element of the array has a width of 0.3 mm, a height of 4 mm, and a center frequency of 7.5 MHz with a 70% bandwidth. The array has an effective length of 46 mm and the pitch between adjacent elements is 0.72mm. The parallel data-acquisition (PDA) equipment is employed to acquire, pretreat and transmit the 64-channel PA signals simultaneously. It contains electronic boards of the receiving module, A/D conversion module, and buffer memory module. In the receiving module, the detected signals are amplified firstly by two-stage amplifiers and then filtered by anti-aliasing filters. In A/D conversion module, analog-to-digital converters with 12-bit precision are equipped. The data sampling rate is 40 M Samples/sec. After A/D conversion, the data from per channel are stored in the buffer memory and finally transferred to the PC through USB interface. With the PDA equipment, the 64-channel array data can be acquired and transmitted every 1/100 second. Thus the frame rate of the PDA equipment is up to 100 Hz, which enable the system to image flowing target. After data acquisition, dynamic focusing reconstruction is applied to reconstruct PA images off-line. Additionally, the PDA equipment is triggered by Q-Switch signal of the Nd: YAG laser.

The linear transducer array has the advantage of plane information collection and we only consider the directivity in the image plane (*X-Y* plane) [22]. The directivity pattern function of individual rectangle transducer can be expressed as follow

$$D(\theta) = \frac{\sin\left(\frac{ka}{2}\sin\theta\right)}{\frac{ka}{2}\sin\theta}, \quad (1)$$

where $k = \frac{2\pi}{\lambda}$ (λ is the ultrasound wavelength), a is the dimension of the width side of the transducer element, θ is the incidence angle of acoustic waves approaching to the transducer. The effective acceptance angle of each transducer element (when $D \geq 1/2$) is equal to 50°.

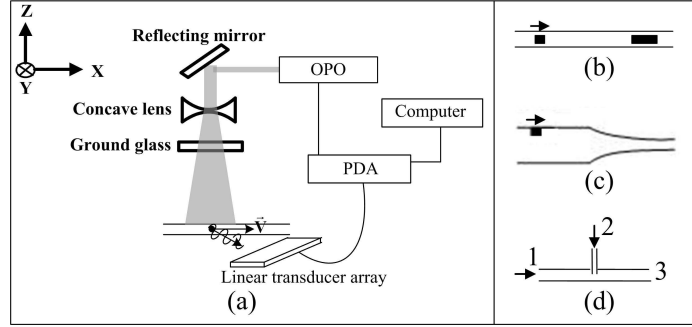


Fig. 1. (a). Schematic of the photoacoustic imaging velocimetry system. PDA: parallel data-acquisition. The light-absorbing target moving along velocity vector is illuminated by laser pulses. The velocity vector is located in the image plane of the linear transducer array. The black circle represents an optical absorber. (b) The schematic of transport apparatus (plastic tube) used in experiment 1 and 2. The black rectangle on the left represents the solid tracer (wood block). The black rectangle on the right represents the mark (a piece of black tape). The arrow shows the direction of flow field. (c) The schematic of the taper glass tube used in experiment 3. (d) The configuration schematic of the tee pipe used in experiment 4 and 5. Port 1 was connected with the infusion pump through the standard syringe to get a constant flow. Port 2 was connected with another syringe and used to inject a small amount of Indian ink. Port 3 was connected with the plastic tube and located in the imaging region.

The limited acceptance angle will induce received heterogeneity for the field of view (FOV) in the processes of data acquisition. Particularly, the effective received accumulation number of points at the edge of the FOV is much less than that of points in the centre of the FOV (When $D \geq 1/2$, we deem it's an effective receive, and add 1 to Ω_{ij} , which is defined as the effective received accumulation number of point (i, j) in the imaging region). The effective received accumulation number is an idealized parameter, and in the paper, it is calculated in the processes of image reconstruction. In reconstruction, if the point (i, j) was located in the effective received angle of m -th transducer, $RF_m(t - \tau_{ij}) \times D(\theta)$ was added to S_{ij} . Simultaneously if $RF_m(t - \tau_{ij}) \times D(\theta)$ was greater than the minimum response value of the transducer, Ω_{ij} was added by 1. For the same absorber at different location of the FOV, the intensity of reconstructed images should be uniform. Thus after focusing reconstruction, in order to modify the received heterogeneity, the pixel value of each point was normalized by the received weighting factor. For the point (i, j) in the imaging region, the image intensity S can be expressed as

$$S_{ij} = w \sum_{m=1}^M [RF_m(t - \tau_{ij}) \times D(\theta)], \quad (2)$$

where RF_m is the received photoacoustic signal by the m -th transducer element, t is the time after the trigger, τ_{ij} corresponds to the acoustic propagation time from the point (i, j) to the m -th transducer element, M is the number of elements in the linear transducer array. w is the received weighting factor and $w = \frac{\Omega_{\max}}{\Omega_{ij}}$, where Ω_{\max} is the maximum of Ω in each individual image.

After modifying the received heterogeneity, the image uniformity in contrast will be changed. For the points in the center area, it can be simply regarded that its PA signal was received absolutely by the linear transducer array. Correspondingly, for the points at the edge

of the FOV, the PA signal was received incompletely. Thus the image intensity in the center of the FOV was used as a standard to assess the improvement of image uniformity in contrast.

After PA reconstruction, an image sequence according time can be acquired, and each image shows the absorbed optical deposit distribution at different time. Thus the dynamic information of moving light-absorbing target can be displayed with the continuous PA images. With the real-time PA imaging method, dynamic information of flow field can be acquired by imaging the moving tracers tracking in the investigated field. To realize imaging velocimetry, the position of the tracer in each reconstructed image should be scaled. In the paper, the centre of the tracer has been used to describe the position simply. And the centre and the size were assessed by the midpoint and the length of the tracer in the moving direction approximately. For accurate measurement, the assessing method of the movement should be developed. The flow velocities were acquired by measuring the movement of the midpoint of tracers. For the liquid tracer in flow field, the variation in length of reconstructed image is used to evaluate the diffusion velocity of the liquid tracer.

In the study, a small rectangular wood block was selected to perform solid absorber. A plastic tube filled with water was used to perform transport apparatus, which has inner diameter of 3 mm and outside diameter of 4 mm with a sound velocity of 2340 m/s. An infusion pump (CZ-74901-15, Cole Parmer VernonHills, IL, USA) and a 1 ml standard syringe connected with the plastic tube were used to produce a constant current. The wood block floated on water, and could be driven by the flow. A piece of black tape glued on the plastic tube was used to mark position. Experiment 1 (Fig. 2) was performed to demonstrate the improved dynamic focusing algorithm (The received heterogeneity is modified) has the ability to modify the received heterogeneity of the FOV. In experiment 1, the wood block was performed as absorber target, and located at the edge and the center of the FOV, respectively. And the transducer array was placed parallel to the plastic tube with a distance of 2 cm. Experiment 2 (Fig. 3) was designed to demonstrate that the PAIV system has the ability to image solid tracer moving in flow field. In experiment 2, the wood block was performed as solid tracer, and a velocity of ~ 1.20 cm/s inside the plastic tube was created by the infusion pump. The schematic of transport apparatus used in the experiment 1 and 2 has been shown in Fig. 1(b). Experiment 3 (Fig. 4) was performed to further demonstrate that the system has the ability to image solid tracer with varying flow velocity. In experiment 3, a taper glass tube was used to produce a varying velocity, and the corner of the taper glass tube was located in the middle of the imaging area. The configuration schematic of the taper glass tube has been shown in Fig. 1(c).

In order to verify that the PAIV system has the ability of whole field flow visualization, Indian ink was performed liquid tracer to track flow field. In experiment 4 (Fig. 5) and 5 (Fig. 6), a tee pipe was used to produce a mixed flow, and the configuration schematic has been shown in Fig. 1(d). Port 1 of the tee pipe was connected with the infusion pump through the standard syringe to get a constant flow. Port 2 was connected with another syringe and used to inject a small amount of Indian ink. The injected ink will diffuse and flow toward port 3 together with the flow from port 1. Port 3 was connected with the plastic tube and located in the FOV. In experiment 4, the transducer array was placed parallel and toward to the flow direction, respectively. In experiment 5, the transducer array was placed obliquely, forming an acute angle with the flow direction. Additionally, the transducer array and the investigated flow direction were also in the same plane. Flow velocity in experiment 5 was 0.20 cm/s.

3. Results

The result of experiment 1 has been shown in Fig. 2. Figure 2(a) and 2(b) are reconstructed PA images with the conventional dynamic focusing algorithm [23,24]. Clearly, the image intensity of the wood block in Fig. 2(a) is weaker than that in Fig. 2(b). Figure 2(c) and 2(d) are reconstructed PA images from the improved dynamic focusing algorithm (The received heterogeneity is modified by the received weighting factor). Obviously, the image intensity of the wood block in Fig. 2(c) is higher than that in Fig. 2(a), while that is almost the same in Fig. 2(b) and 2(d). The reconstruction profiles of the wood block from Fig. 2(a)-2(d) with $y =$

11.5mm have been shown in Fig. 2(e) with different color. The mean relative intensity of the wood block is 853, 1164, 1062 and 1164 (a.u.), respectively. Approximately, 18% improvement of image uniformity in contrast is reached by modifying the received heterogeneity.

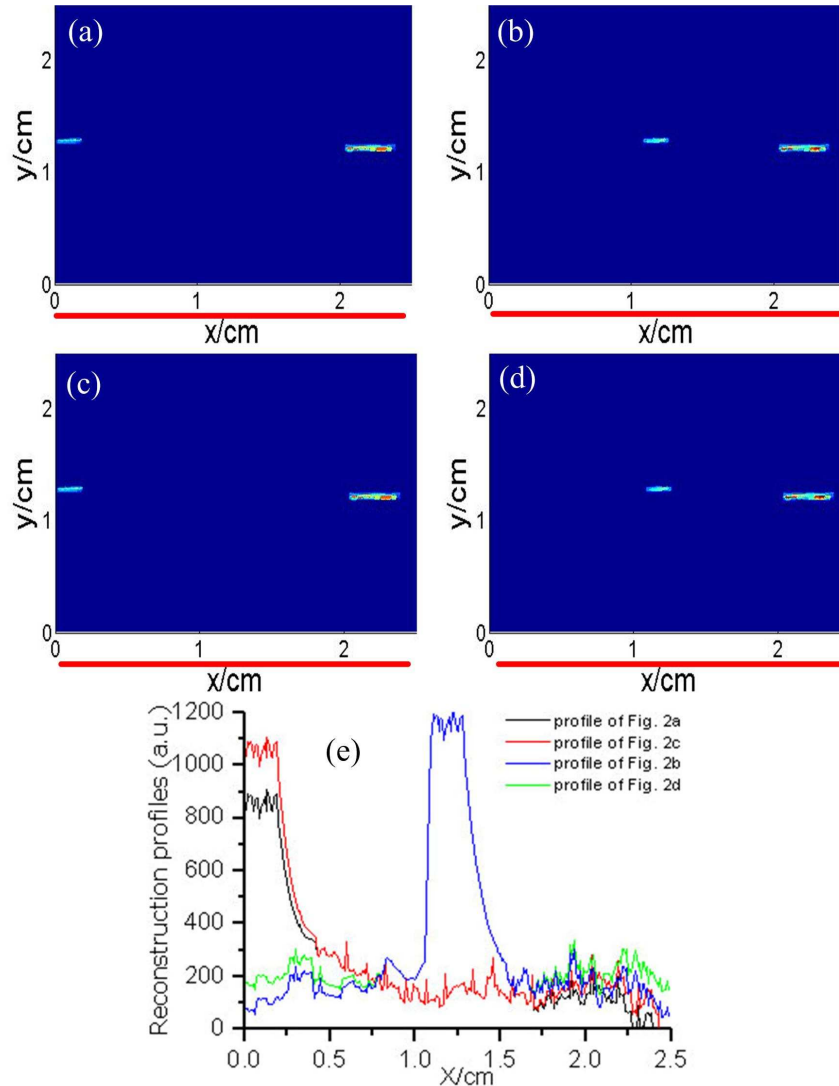


Fig. 2. Reconstructed photoacoustic images with the wood block located at different position of the FOV. (a) and (b) Reconstructed PA images from the conventional dynamic focusing algorithm with the absorber target located at the edge and in the centre of the imaging area, respectively. (c) and (d) Reconstructed PA images from the improved dynamic focusing algorithm modified with the received weighting factor. (e) Reconstructed profiles at $y = 11.5$ mm of images (a)-(d). The reconstruction profiles of the wood block from (a)-(d) are shown with the color of black, blue, red and green, respectively. The red line in each panel represents the position of the linear transducer array.

After modifying the received heterogeneity, image intensity of the wood block at the edge of the FOV is closer to that in the center of the FOV. Thus we believe that Fig. 2(c) is more uniform in contrast of whole image than 2(a). Image intensities of the wood block in Fig. 2(b) and 2(d) are almost identical, and the reason is that in the center of the FOV the received weighting factor w is almost equal to 1. Additionally, it is hard to eliminate the heterogeneity

of the FOV completely, and another reason should be the inhomogeneous light due to the heterogeneity of light energy distribution. In conclusion, after modifying the received heterogeneity, the intensity of absorber at the edge of the FOV has been more close to that in the center of the FOV. In conclusion, with the improved dynamic focusing algorithm, a relative homogeneous imaging area can be obtained.

In experiment 2, the movement of the tracer with constant velocity was captured in 2.06 second. Reconstructed result has been shown in Fig. 3 with an interval of 0.33 second. There are two absorbers in the reconstructed images. The shorter one is the tracer moving with the flow field, and the longer one at the right of the reconstructed images is the marker. The distances traveled between successive images in Fig. 3 are 3.7mm, 3.8mm, 3.8mm, 4.1mm, 3.9mm and 4.3mm, respectively. And the average velocity of the tracer is 1.18 cm/s. The experiment result demonstrates that the PAIV system has the ability of flow visualization for moving target. In the experiment, the velocity of flow field is evaluated by measuring the movement of the solid tracer. Solid tracer is driven by the investigated flow in this measuring mode, thus small and low-density tracer should be selected.

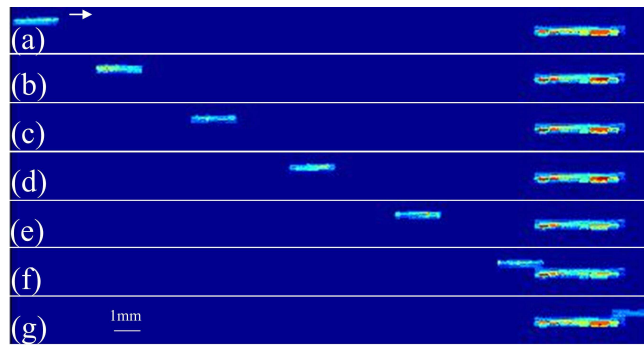


Fig. 3. PA images of the solid tracer with constant velocity at different times. The movement of the tracer was captured in 2.06 second. The arrow shows the direction of flow field. The red line represents the position of the linear transducer array.

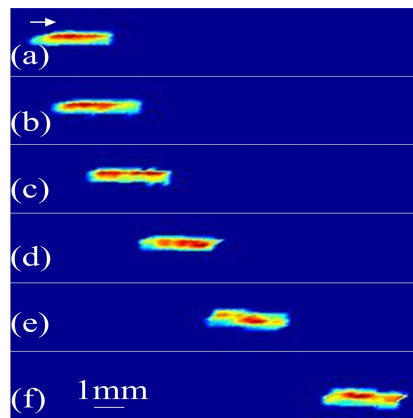


Fig. 4. PA images of the solid tracer with varying velocity at different times. The movement of the tracer was captured in 1.06 second. The arrow shows the direction of flow field. The red line represents the position of the linear transducer array.

Result of experiment 3 has been shown in Fig. 4 according to time with an interval of 0.2 second. Seen from Figs. 4(a) to 4(c), it is clearly that the velocity of the tracer is homologous. While seen from Figs. 4(d) to 4(f), distance traveled between successive images is enlarged gradually, which means that the velocity of the tracer is varied. Furthermore, it also can be observed that moving direction of the tracer has been changed from Figs. 4(d) to 4(f), which is

caused by the corner of the tube. It is further demonstrated that the PAIV system has the ability of flow visualization for flow field.

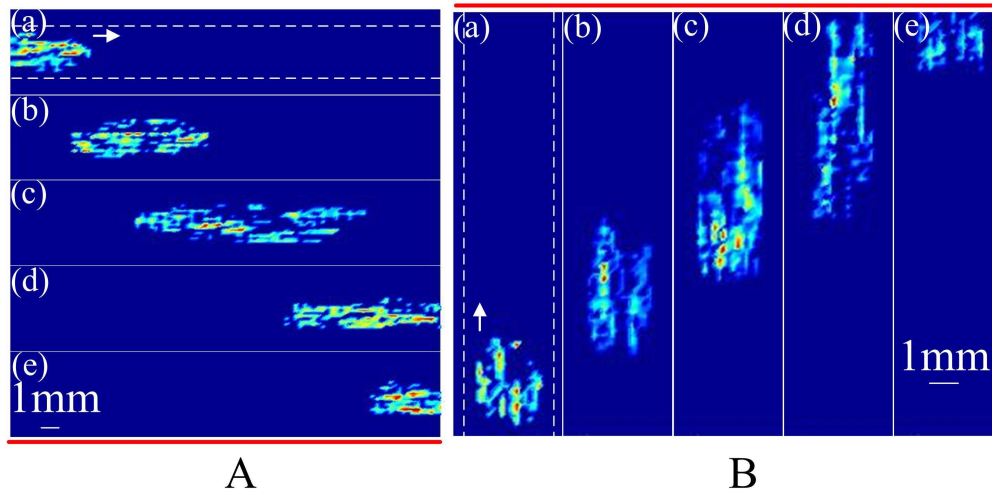


Fig. 5. PA images of liquid tracer at different times. The dash lines represent positions of the wall of the plastic tube. Arrows show the flow direction. A: The transducer array was placed parallel to the flow direction. The movement of the liquid tracer was captured in 1.06 second. B: The transducer array was placed toward to the flow direction. The movement of the liquid tracer was captured in 1.66 second. The red line represents the position of the linear transducer array.

Reconstructed PA images of experiment 4 are shown in Fig. 5. In Fig. 5A, images (a)-(e) are given according to time with an interval of 0.2 second. It is shown that the liquid tracer is flowing from left to right. In Fig. 5B, images (a)-(e) are given in time sequence and the time interval is 0.4 second. It is shown that, the liquid tracer is flowing toward to the transducer array. In Fig. 5, the moving direction of the liquid tracer is accurately acquired, and the diffuseness phenomenon is also clearly displayed. In the diffusion process, the ink will be affected by the adhesion force of flow and can't maintain a fixed shape. Thus reconstructed PA images of the liquid tracer are different with time. In the experiment, the ever-changing liquid tracer is imaged real-timely, which demonstrates that the PAIV system has the ability of whole field flow visualization.

Figure 6 shows the reconstructed PA images of the liquid tracer with an oblique direction toward the transducer array in experiment 5. Images (a)-(f) are given according to time with an interval of 0.2 second. Furthermore, flow velocity and diffusion velocity of the liquid tracer are measured from successive PA images. The mean flow velocity is 0.17 cm/s and the mean diffusion velocity is 0.07 cm/s in the experiment. It is demonstrated that the PAIV system has the ability to acquire the flow direction information. In the experiment, the random flow direction was limited in a plane, which was caused by the plane information selection of the linear transducer array.

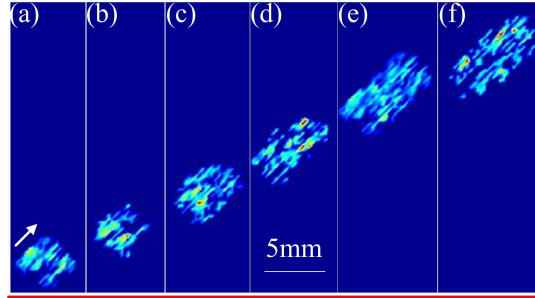


Fig. 6. PA images of liquid tracer in a flow with an oblique direction toward the transducer array. The movement of the tracer was captured in 2 second. The red line represents the position of the linear transducer array.

4. Discussion and conclusion

We have presented the photoacoustic imaging velocimetry method for flow field measurement. Present work has demonstrated that the system has the ability of 2-D flow visualization. Furthermore, both velocity and direction of the investigated flow can be obtained from reconstructed PA images. The current system can only be used in 2-D measurement, which is limited by the plane-selected transducer array. For 3-D measurement, a planar array with large 3-D acceptance angle and appropriate structure is needed, and this is our further work. The frame rate of the PAIV system is limited by the low pulse repetition frequency (PRF) of the laser, and the time resolution of the system is restricted.

Actually, in the PAIV measurement sound velocity v_0 of PA wave will be affected by the flow field [25]. Assuming that the flow is moving away from the transducer with a velocity v (In this case, the speed of sound deviation is maximum), the sound velocity will be $v_0 - v$,

and the relative error of the target location can be described as $\frac{v}{v_0 - v}$. If 1% is selected to

perform the limit of the relative error, the maximum measuring velocity of the PAIV method is about 14.85 m/s (Assuming that the sound speed is equal to 1500 m/s). In practical medical application, the sound velocity will change throughout the medium. In this case, the measured relative velocity can be used to evaluate flow field qualitatively, and the dynamic information is also useful for clinic diagnosis. For further development, investigated velocity can be acquired by correcting the acoustic speed variations with ultrasonic transmission tomography [26]. For the current imaging system, the actual limiting velocity is well below the maximum measuring velocity due to the low pulse repetition frequency (PRF) of the laser. Previously, a 1 kHz repetition laser has been used in PA imaging by Wang et al [27]. With high pulse repetition frequency laser in future, the PAIV system can overcome the current limiting velocity.

The light scattering will result in: (1) the light energy distribution will be more homogeneous, which will induce a more homogeneous imaging area; (2) the light energy will be decreased. For the reconstructed image, the image intensity will be decreased. However, in the paper the imaging area was located in a plane and was almost vertical with the light. Thus the affection of the image intensity due to the light scattering can be neglected.

In the processes of image reconstruction, Ω_{ij} was accumulated when $D \geq 1/2$ and $RF_m(t - \tau_{ij}) \times D(\theta)$ was greater than the minimum response value of the transducer. For the white noise at the edge of the FOV, the accumulation number Ω_{ij} is possible less than that of sharp absorber at the same position, and correspondingly the parameter w should be great. Thus in the same region the improvement value of Figs. 2(b) and 2(d) is not the same as

that in Figs. 2(a) and 2(c). For the same point in different image, the parameter Ω would be different, thus the range in each image with the parameter w is almost equal to 1 is different with each other. Only when the parameter w is almost equal to 1, the lines before and after modifying the received heterogeneity can coincide with each other. This should be the reason why the coinciding range of the green line and the blue line is different with that of the black line and the red line.

The PAIV method has some advantages for flow field measurement. 1) Compared to Doppler flow imaging (laser Doppler imaging and ultrasound Doppler imaging) [28,29], the PAIV method can provide the direction information of the investigated velocity vector, while the measured velocity by Doppler flow imaging is just a projection of the investigated velocity vector in the probe direction. 2) Compared to speckle contrast flow imaging (SCFI) and particle imaging velocimetry (PIV) [30,31], the PAIV method possesses a better sensitivity. With a single probe (light or sound), SCFI and PIV are based on the scattering property of endogenous red blood cells or exogenous particles. However, the light is strongly scattered by the tissue and the ultrasound wave is strongly reflected by tissue boundaries [32]. On the contrary, PAI employs both light and sound as probe and relies on light absorption contrast. 3) The PAIV method can provide more information of the investigated flow field except mean flow velocity. The measuring region of the imaging system is a large area, not a point. Thus the method can be used to display the varying flow.

The method would be regarded as a new scientific research method, and potentially applied in the research of security and targeting efficiency of optical nano-material probes. Recent year, more and more attention has been attracted in nanotechnology research. And the optical nano-material probes, such as carbon tubes probe [33], golden carbon tubes probe [34], have been tried to target and identify tumor. However, the penetration and the targeting efficiency of the nanoparticles should be assessed experimentally. With the photoacoustic imaging velocimetry method, the movement of optical nano-material probe could be monitored realtimely. By mapping of the dynamic distribution of optical nano-material probe, the penetration and flow tendency could be observed clearly, and the targeting efficiency could be obtained by monitoring the PA intensity of the particles around the tumor.

In conclusion, we have developed the photoacoustic imaging velocimetry method for flow field measurement. The method can be developed into 3-D imaging velocimetry. The photoacoustic imaging velocimetry system was presented and its ability of visualizing and measuring flow has been demonstrated experimentally.

Acknowledgements

This research is supported by the National Basic Research Program of China (2010CB732602), the Program for Changjiang Scholars and Innovative Research Team in University (IRT0829), the National Natural Science Foundation of China (30627003; 30870676), and the Natural Science Foundation of Guangdong Province (7117865).